

Investigation Of Crystallisation Conditions to Produce CL-20/HMX Cocrystal for Polymer-bonded Explosives

Dirk Herrmannsdörfer,^{*,[a]} Peter Gerber,^[a] Thomas Heintz,^[a] Michael J. Herrmann,^[a] and Thomas M. Klapötke^[b]

Abstract: Since its discovery in 2012, multiple techniques to generate the CL-20/HMX cocrystal have been published. However, as yet no assessment or trial has been reported of crystallisation methods capable of producing the cocrystal in a size region and production scale suitable for its use in polymer bonded explosives (PBX). This paper provides insight into the selection of suitable crystallisation methods, solvent selection and process optimisation with a focus on the efficient production of high-quality cocrystals for use in PBX. Through extensive solvent screening, acetonitrile was identified as the best solvent for solution-based crystal-

lisation, due to its capability to produce compact parallelepipedic crystals and its comparably wide cocrystal phase region. Crystallisation conducted at 60 °C was found to increase the conversion rate and the material efficiency compared to room temperature. By application of an advanced seeding procedure, high-quality cocrystals in the size region of 180–250 µm were produced in laboratory-scale anti-solvent and cooling crystallisations. By pilot-plant-scale batch reaction cocrystallization, cocrystals with a volume-weighted mean diameter of 33 µm were produced in quantities of 250 g per day.

Keywords: Cocrystal • CL-20 • Energetic material • HMX

1 Introduction

2,4,6,8,10,12-hexanitro-2,4,6,8,10,12-hexaazaisowurtzitane (CL-20) outperforms 1,3,5,7-tetranitro-1,3,5,7-tetracyclooctane (HMX) in terms of detonation velocity, oxygen balance, and explosive power [1,2]. However, it has not seen any widespread use in high explosives formulations because of its comparably high mechanical sensitivity [2,3,4].


One way to approach the sensitivity issue of CL-20 was presented by Bolton *et al.* in the form of the 2:1 CL-20/HMX cocrystal [3]. There is still ongoing debate in the scientific community about what kind of species should be called cocrystals [5,6]. Here we adopt the proposed definition of Aitipamula *et al.* [5] “cocrystals are solids that are crystalline single-phase materials composed of two or more different molecular and/or ionic compounds generally in a stoichiometric ratio” knowing that this definition partly overlaps with the definitions of salts and solvates. The CL-20/HMX cocrystal is reported to possess comparable impact sensitivity to HMX and to exceed HMX in terms of detonation velocity. [3] This cocrystal is therefore a promising candidate to succeed HMX as the state-of-the-art high explosive. Multiple techniques are presented in the literature to generate the cocrystal: Antisolvent crystallisation [7], spray flash evaporation [8], spray drying [9], solvent evaporation [3,10,11], ultrasonic spray-assisted electrostatic adsorption [12], liquid-assisted grinding [3,7,13], and reaction cocrystallisation [10]. The term reaction cocrystallization (RC) was coined by Rodríguez-Hornedo *et al.* [14] and describes co-

crystallisation utilising the solubility difference between the cocrystal and the individual cocrystal components. For use of the cocrystal in PBX, special requirements concerning morphology and crystal size distribution need to be achieved in order to ensure processability of the PBX. The following product parameters were therefore chosen:

- Crystals of compact morphology are beneficial to the processability of the PBX, due to the detrimental effect of plate-like particles on the viscosity.
- A crystal size distribution with a volume-weighted mean diameter (d_m) in the region of 200 µm must be accessible, as the desired explosive loadings of 85–90 % typically require the application of a bimodal particle size distribution that is separated by one order of magnitude. The application of very fine crystals in the PBX can lead

[a] D. Herrmannsdörfer, P. Gerber, T. Heintz, M. J. Herrmann
Energetic Materials
Fraunhofer Institute for Chemical Technology ICT
Joseph-von-Fraunhofer-Str. 7
76327 Pfinztal, Germany
Fax: (+)49 (721) 4640-111
*e-mail: dirk.herrmannsdorfer@ict.fraunhofer.de

[b] T. M. Klapötke
Department of Chemistry
Energetic Materials Research
Ludwig-Maximilian University of Munich
Butenandtstr. 5–13 (Haus D)
81377 Munich, Germany

 Supporting information for this article is available on the WWW under <https://doi.org/10.1002/prop.201800332>

to an undesirably high viscosity. For this reason a pairing of 20 μm and 200 μm for d_m is often the target.

- As sensitivity to shock and impact tends to depend on crystal quality (gas/liquid inclusions, voids, dislocations,...) [15], a crystallisation process capable of producing high-quality crystals is preferred.
- Due to the cost of CL-20, the crystallisation method must either exhibit a good CL-20 efficiency or CL-20 must be easily recyclable from solution.

Based on the defined product parameters, the list of applicable crystallisation methods narrows down to anti-solvent crystallisation, cooling crystallisation, reaction co-crystallization and evaporation crystallisation, since other methods generally offer only limited options to control crystal size and crystal quality. In this paper we describe the steps needed to develop a cocrystallisation process capable of producing CL-20/HMX cocrystals in the 100 g range with tuneable crystal size, compact morphology and high crystal quality. In particular, the following four steps are presented:

- Definition of product parameters
- Selection of crystallisation process
- Solvent selection
- Optimisation of process parameters

2 Experimental Section

All solvents were reaction grade or higher and were stored over 3 Å molecular sieve. CL-20 (lot number 573598) was obtained from SNPE. HMX (lot number NSI 00E 000 E004) was purchased from Chemring Nobel.

2.1 Characterisation Methods

Raman spectra were obtained with a Bruker RFS 100/S Raman spectrometer equipped with a 1064 nm ND:YAG-laser operated at 450 mW and a liquid-nitrogen-cooled Germanium-detector. The spectra were obtained between 80 and 3500 cm^{-1} with a spectral resolution of 1 cm^{-1} .

X-ray powder diffraction measurements were performed on a D8 Advance from Bruker AXS, equipped with a copper tube, two 2.5° Soller collimators, an anti-scatter screen, a flip-stick stage, and a silicon strip detector (LynxEye). The data was evaluated using Rietveld analysis based on the structure data reported by Bolton *et al.* [3].

Macroscopic images were taken with a Leica DFC420 camera equipped with a Leica Z16APO objective. The images were processed via Leica QWin V3 software.

Particle diameters were determined with a Malvern Mastersizer 2000 version 5.60 with a heptane-lecithin mixture as a dispersion medium. The agitation speed was 2450 rpm. Prior to every measurement, injected samples were ultrasonicated for 2 minutes with 60% intensity. 1.69 was chosen as the refractive index and the absorption coefficient was selected individually to obtain the best results. Three

measurements, each consisting of 10000 individual scans, were averaged.

HPLC measurements were performed with an Agilent 1100 equipped with binary pumps and a diode array detector detecting at 225 nm. A Kintex 2.6 μm C18 100 Å 100 × 4.6 mm column with a Phenomenex precolumn was used with water:acetonitrile (1:1) as eluent at a flow rate of 0.6 mL min^{-1} at a column temperature of 35 °C. Analysis was carried out using a ChemStation for LC 3D systems Rev. B.01.03.

Laboratory-scale experiments were agitated and temperature controlled using a Ditabis MKR 23 thermo block mixer equipped with a matching thermo block for the reaction vessels.

2.2 Solubility Determination

A moderate excess of HMX or CL-20 was placed in a 6 mL glass vessel. Depending on the expected solubility, between 0.5 g and 3 g solvent were added. The solution was agitated at 800 rpm and tempered via a Ditabis MKR 23 thermo block mixer equipped with a matching thermo block for the reaction vessels for 5 hours. The solid was sedimented and the clear solution removed by syringe. Directly afterwards the solution mass was determined. The solvent was removed under vacuum and the mass of the remaining solid was determined.

2.3 Standard Washing Procedure

The product solid phase of laboratory-scale crystallisation experiments was washed consecutively with three solutions with decreasing solubilities of CL-20 and HMX to avoid precipitation from the solution and excess dissolution of the solid. The typical washing procedure was 1 mL 2-propanol:acetonitrile (8:2), 1 mL 2-propanol:acetonitrile (9:1), and 5–10 times 1 mL 2-propanol.

2.4 Phase Solubility Diagram

The phase diagrams were obtained via the static method [16]. For PC and DMC, excess CL-20 and HMX was agitated at 800 rpm and 60 °C. Typically 1 g of solvent was used. All slurries were seeded with cocrystal after 5 h. After at least 5 d the solid was sedimented and an aliquot of the clear solution was removed by syringe and diluted with acetonitrile (ACN). The CL-20 and HMX concentrations were measured by HPLC. The solid phase was washed according to the standard washing procedure. The solid phase was characterised by Raman spectroscopy.

For ACN at 60 °C and 20 °C, and ACN:2-propanol (1:1) mixture, DMC and butane-2,3-dione at 60 °C, excess CL-20 and cocrystal was agitated at 800 rpm and no additional

seeding was carried out. Except for the substitution of HMX by cocrystal, the previously described procedure was applied. The altered procedure was intended to eliminate the need for additional seeding and, in the case of DMC and butane-2,3-dione, ensure that slow cocrystallisation rates did not hinder the equilibration.

2.5 Seeding Procedures

In self-seeded laboratory-scale experiments the super-saturated mixture was agitated at 800 rpm at 60 °C for 24 h before antisolvent was added. Over the 24 h period, large crystals (500–700 μm) formed because of the moderate supersaturation (1.2) and thus low nucleation rate. The large crystals were rounded during the process due to the agitation. The fragments acted as seed crystals in the subsequent crystallisation.

In externally seeded laboratory-scale experiments 500 mg ACN (12.2 mmol) was added to 6.4 mg HMX (22 μmol) and 221.6 mg CL-20 (505.7 μmol) in a 6 mL glass vessel. The solid was dissolved at 70 °C and 800 rpm for 10 minutes to ensure total dissolution of CL-20 and HMX. In preliminary experiments, it was found that overheating the crystallisation solution by 10 °C increases the metastable zone width, so that without seeding no crystallisation occurs during antisolvent and cooling crystallisations. Subsequently, the solution was cooled to 20 °C, 5.0 mg cocrystal was added and the dispersion agitated at 800 rpm for 10 minutes. By this method 90% of the seed crystal mass was dissolved and the seed crystals gained a fresh surface with few defects. 60 μL of this suspension were swiftly transferred to the previously prepared reaction solution using a 20–200 μL VWR Collection Standard Line single channel mechanical air displacement micropipette.

In seeded RC experiments no HMX was used in the seed solution and accordingly more cocrystal was used. Furthermore, the reaction mixture was not heated to 70 °C.

2.6 Antisolvent Crystallisation

3000 mg ACN (73.08 mmol) was added to 152 mg HMX (0.51 mmol) and 1472 mg CL-20 (3.36 mmol) in 20 mL glass vessels. The solid was dissolved at 70 °C and 800 rpm for 10 minutes. Subsequently, the solution was cooled to 60 °C. The seed crystal suspension was added and the reaction vessels were air-tightly connected to the pump tube via teflon fittings. 2000 mg 2-propanol (33.27 mmol) was dispensed over the course of 16.6 h using a Hirschmann ROTARUS VOLUME 50I metering pump equipped with a ROTARUS MKF 12-8 12 channel pump head. During crystallisation the temperature was kept constant at 60 °C and the vessels were agitated at 600 rpm. The solid phase was washed according to the standard washing procedure. Ev-

ery experiment was carried out in parallel at least threefold. The solid phase was characterised by Raman spectroscopy.

For internally seeded and unseeded crystallisation experiments in ACN no heating to 70 °C and no addition of seed crystal suspension was undertaken.

For crystallisation experiments in propylene carbonate the same procedure was applied as in unseeded crystallisation experiments in ACN, except that 3000 mg propylene carbonate (29.39 mmol), 123 mg HMX (0.42 mmol) and 1276 mg CL-20 (2.91 mmol) were used.

2.7 Cooling Crystallisation

3000 mg ACN (73.08 mmol) was added to 152 mg HMX (0.51 mmol) and 1472 mg CL-20 (3.36 mmol) in a 20 mL glass vessel. The solid was dissolved at 70 °C and 800 rpm for 10 minutes. Subsequently, the solution was cooled to 60 °C. The seed solution was added. During the crystallisation the temperature was decreased to 20 °C over the period of 5 to 30 h following a progressive or natural cooling curve. The vessels were agitated at 800 rpm. The solid phase was washed according to the standard washing procedure. Every experiment was carried out in parallel at least threefold. The solid phase was characterised by Raman spectroscopy.

For cooling crystallisation with adapted solution composition, 119 mg HMX (0.40 mmol) and 1472 mg CL-20 (3.72 mg) was used. Linear cooling over the period of 16.6 h and natural cooling over the period of 25 h was applied.

2.8 Batch Reaction Cocrystallization

In intermediate-scale crystallisation experiments carried out in ACN at 20 °C, ACN at 60 °C and cyclohexanone at 60 °C the excess of solid was chosen as 600 mg mL^{-1} of solution. This choice was made to ensure comparability between the solvents. The experiments were agitated using a CAT R60 overhead stirrer fitted with a 3 cm three-blade propeller stirrer, and temperature controlled using a Lauda RC6 CP thermostat fitted to the 50 mL jacketed reaction vessel. For ACN at 20 °C 13.30 g ACN (324.0 mmol) was added to 2.172 g HMX (7.33 mmol) and 12.373 g CL-20 (28.24 mmol). For ACN at 60 °C 13.30 g ACN (324.0 mmol) was added to 2.275 g HMX (7.68 mmol) and 14.577 g CL-20 (33.27 mmol). For cyclohexanone at 60 °C 14.50 g cyclohexanone (147.7 mmol) was added to 2.148 g HMX (7.26 mmol) and 15.686 g CL-20 (35.79 mmol). The reaction mixture was agitated at 440 rpm. An aliquot of 400 μL of seed slurry prepared from 0.500 g cyclohexanone (5.09 mmol), 0.0240 g cocrystal and 0.329 g CL-20 (0.75 mmol) was added to the cyclohexanone slurry after 3 h. After 2 h or 18 h for ACN at 20 °C, 1 h for ACN at 60 °C and 18 h for cyclohexanone, the stirrer was removed and the slurry transferred into a Büchner funnel using a BRAUN omnifix 100 mL syringe without a cannula at-

tached to avoid clogging. The mother liquor was removed and the product crystals were washed with 10 mL 2-propanol:ACN (8:2), 30 mL 2-propanol:ACN (9:1) and five times with 10 mL 2-propanol to ensure the total removal of the mother liquor. The product crystals were dried under vacuum and Raman spectra were collected to determine the purity.

The pilot plant crystallisation was carried out in three consecutive batches. The mother liquor of the first batch was reused in the second as well as the third batch. With each filtration process to remove the product crystals mother liquor is lost. To compensate, with each batch the solid load was reduced by 10 g, and 1 g of ACN was added. For the first batch 80.0 g (1.95 mol) ACN was added to 28.0 g HMX (94.5 mmol) and 112.0 g (255.6 mmol) CL-20 in a 250 mL jacketed flask with a rounded bottom. The slurry was agitated at 240 rpm for 2 h at 60 °C via an overhead stirrer equipped with a paddle stirrer. The stirrer's contour closely matches the inner wall contour of the jacketed vessel. After 2 h the stirrer was removed and the slurry was transferred into a Büchner funnel using a BRAUN omnifix 100 mL syringe without a cannula attached to avoid clogging. After the removal of the mother liquor, the suction filter was moved to another vacuum side-arm flask, the mother liquor was transferred back into the reaction vessel, and the product crystals washed with 30 mL 1:1 2-propanol:ACN, 30 mL 2-propanol:ACN (8:2), 30 mL 2-propanol:ACN (9:1), 30 mL 2-propanol (two times) and 100 mL 2-propanol (once) to ensure the total removal of the mother liquor. The same procedure was applied for batch 2 and 3, but using 22.5 g (76.0 mmol) HMX and 67.5 g (154 mmol) CL-20, and 20.0 g (67.5 mmol) HMX and 60.0 g (137 mmol) CL-20 respectively. The product crystals were dried under vacuum and Raman and XRD measurements were carried out to determine the purity.

3 Results and Discussion

3.1 Solvent Selection

3.1.1 Solubility

The solubilities of HMX and CL-20 play an important role in the selected crystallisation methods. The CL-20/HMX cocrystal is composed of two parts CL-20 per part HMX and the molecular mass of CL-20 is approximately 1.5 times the molecular mass of HMX. Hence, as a first approach to identify a suitable solvent for cocrystallisation, a solvent was sought which exhibits a three times better solubility of CL-20 than HMX, because it is reasonable to assume that a better solubility ratio corresponds to a more favourable cocrystal phase region in the ternary phase diagram [17]. Once a matching solvent is identified, the cocrystal phase region could be determined. Based on the available solubility data [18], it was concluded that HMX is always far less soluble

than CL-20, and exhibits a temperature-dependent solubility. Based on these findings, solubility screenings were conducted at 20 °C and 60 °C. The upper temperature was chosen as a compromise between the better solubility values for HMX at higher temperatures, safety concerns and the limiting factor of boiling point. A detailed analysis of the gathered solubility data will be published elsewhere. For this work it suffices to state that CL-20 did not exhibit a significant temperature-dependent solubility. The best solubility ratios of CL-20 and HMX were therefore obtained at 60 °C. The twelve solvents with the best solubility ratio at 60 °C are listed in Table 1.

Table 1. Solubilities of CL-20 and HMX with solubility ratios in different solvents at 60 °C.

	[HMX] (g/g solvent)	[CL-20] (g/g solvent)	Solubility ratio
ACN	0.049	1.372	28
β-butyrolactone	0.073	0.892	12
butane-2,3-dione	0.006	0.068	11
cyclohexanone	0.051	0.859	17
dimethyl carbonate	0.006	0.044	7
ε-caprolactone	0.137	0.9–1.4 ^a	7–10
formic acid	0.001	0.007	7
γ-heptalactone	0.060	0.721	12
γ-hexalactone	0.095	0.910	10
propylene carbonate	0.092	0.841	9
thiophene	0.001	0.004	4
tetramethylurea	0.184	1.285	7

a) Extrapolated value from diluted solution, due to excessive viscosity.

Of these solvents ε-caprolactone was excluded from further studies due to its high solution viscosity. Formic acid and thiophene were neglected because of their low solubility.

3.1.2 Cocrystal Analysis

Raman spectra were obtained from all crystallisation experiments. The product composition was determined via reconstruction of the recorded spectra with pure sample spectra of CL-20, HMX and cocrystal. Unless specifically indicated, all the following crystallisations yielded pure cocrystal.

3.1.3 Cocrystal Formation

As the ternary phase diagram of HMX, CL-20 and solvent was unknown for all solvents, the solubility data of pure CL-20 and HMX (Table 1) for the solvents in question was used as the solution composition to determine the capability of the solvent to produce cocrystal. In unseeded experiments all

solvents with the exception of dimethyl carbonate, butane-2,3-dione and tetramethylurea produced pure cocrystal within 72 h. Dimethyl carbonate produced a mixture of β HMX and ϵ CL-20, butane-2,3-dione produced β CL-20, and in tetramethylurea cocrystal formation as well as a partial decomposition of CL-20 took place, which led to a red discoloration of the solution and gas development. The decomposition is not unexpected due to the incompatibility of CL-20 and amines [19]. To eliminate the possibility that slow conversion into the cocrystal was the reason for the non-conversion in butane-2,3-dione and dimethyl carbonate, phase diagram determinations starting with excess cocrystal were carried out. Dimethyl carbonate and butane-2,3-dione again produced a respective mixture of β HMX and ϵ CL-20, and of β HMX, β CL-20, ϵ CL-20 and cocrystal after 72 h. Given these seemingly contradicting results for butane-2,3-dione, a mixture of excess HMX and excess CL-20 in butane-2,3-dione was agitated at 60 °C for 14 d. Here a mixture of ϵ CL-20 and cocrystal was obtained. These results might indicate a complex phase diagram and low conversion rates in this solvent, which are both undesirable attributes for the cocrystallisation. Due to their adverse properties butane-2,3-dione, dimethyl carbonate and tetramethylurea were eliminated from consideration for cocrystallisation and no further experiments were carried out with these solvents.

3.1.4 Morphology

In the preliminary tests three basic cocrystal morphologies were obtained (Figure 1). β -butyrolactone, γ -heptalactone, γ -hexalactone and propylene carbonate produced elongated hexagonal plate-like crystals, cyclohexanone produced irregular capped parallelepipedic crystals, and ACN, butane-2,3-dione and tetramethylurea produced parallelepipedic crystals. Representative images of the cocrystals

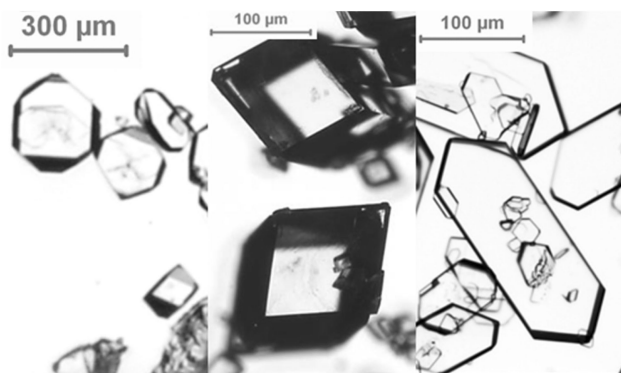


Figure 1. Morphology of cocrystals obtained from cyclohexanone (left); morphology of cocrystals obtained from ACN, butane-2,3-dione and tetramethylurea (centre) and morphology of cocrystals obtained from β -butyrolactone, γ -heptalactone, γ -hexalactone and propylene carbonate (right).

obtained for all tested solvents are found in the supporting information.

The approximate width-to-height ratios derived from macroscopic images is summarised in Table 2. The longest distance between two parallel sides of the largest crystal face was chosen as the width. The ratio values are strongly dependent on the crystallisation condition [3] and are only used as a rough estimate to judge the merit of a solvent.

Table 2. Width-to-height ratios of cocrystal obtained from different solvents.

	Width-to-height ratio
ACN	2
β -butyrolactone	8
butane-2,3-dione	3
cyclohexanone	2
γ -heptalactone	8
γ -hexalactone	8
propylene carbonate	6
tetramethylurea	> 10 ^a

^a estimated value – as the plates were so thin, no side view was achievable.

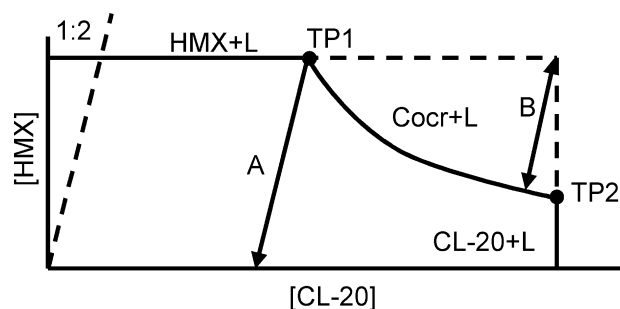


Figure 2. Schematic phase solubility diagram for a system where cocrystal is more soluble than HMX.

The hexagonal elongated shape of the crystals produced in β -butyrolactone, γ -heptalactone, γ -hexalactone and propylene carbonate is undesirable. As the crystal habit can change with the crystallisation conditions [20], propylene carbonate was chosen for further studies. Of the four solvents, it possesses the best solubility and width-to-height ratio. Thus the only remaining solvents for consideration are ACN, cyclohexanone and propylene carbonate.

3.1.5 Transition Concentration

Even though a phase diagram only represents equilibrium conditions, and crystallisation occurs under non-equilibrium conditions, the phase diagram is a powerful tool for finding optimal crystallisation conditions. The phase solubility diagram (PSD, Figure 2) describes the regions of thermody-

dynamic stability of the cocrystal and the individual components. The transition points (TP1, TP2, Figure 2) [16,21] are the boundaries of the cocrystal phase region at which the solution, the solid cocrystal and one solid individual component are in thermodynamic equilibrium. The concentrations in Figure 2 are expressed in terms of moles of CL-20 or HMX per gram solvent. The diagonal dashed line therefore indicates the stoichiometric composition of the cocrystal. Figure 2 illustrates the case where the cocrystal has a higher solubility than HMX in pure solvent. Ideally the cocrystal should be less soluble than the reactants, because the cocrystal is only the thermodynamically favoured crystallisation product within the cocrystal phase region. In that case the cocrystal can be formed from solution of a 2:1 CL-20:HMX stoichiometric composition and no excess of one of the two is required. Where the cocrystal is more soluble than one of the components a TP as close as possible to the stoichiometric composition of the cocrystal is preferred, as that minimises the excess of one of the components needed to reach the cocrystal phase region.

In ACN, cyclohexanone and propylene carbonate the cocrystal is more soluble than HMX. Hence the TP1 serves as an indicator for the quality of the solvent. The TP1 values for the three solvents and the corresponding solubility ratios are summarised in Table 3.

Table 3. Solution concentrations with solubility ratio of CL-20 and HMX at TP1 in different solvents at 60 °C.

	TP1 [HMX] (g/g _{solvent})	[CL-20] (g/g _{solvent})	Solubility ratio at TP1
ACN	0.054	0.424	8
cyclohexanone	0.015	0.605	40
propylene carbonate	0.060	0.374	6

The TP1 solubility ratios do not correlate well with the solubility ratios presented in Table 1. In cyclohexanone and propylene carbonate the HMX solubility decreases with increasing CL-20, while in ACN the HMX solubility increases. It is apparent that besides the solubility of the pure cocrystal components, their interaction in solution plays an important role in determining the position of the cocrystal phase region. The solubility data of the pure cocrystal components can therefore only act as a rough tool for judging the merit of a solvent. The implications of these TP1 values for the applicability of the solvents in the different crystallisation methods need to be individually addressed, due to the fundamental differences in the crystallisation techniques.

In antisolvent and cooling crystallisation the supersaturation is generated by the transition from a cocrystal phase region of higher solubility to a cocrystal phase region of lower solubility, either by adding an antisolvent or by cooling. For maximal efficiency of the process a large differ-

ence in solubility between the two phase regions is required. As the solubility of the cocrystal is higher than the solubility of HMX in all three solvents, the maximum possible yield of cocrystal per gram solvent is determined by the TP1 HMX solubility. In Table 4 the theoretical maximum yield of cocrystal for the three solvents for cooling and antisolvent crystallisation is summarised under the simplification that the final HMX solubility in any case is zero (arrow A in Figure 2). Additionally, the corresponding CL-20 efficiencies are presented in Table 4, i.e. the ratio of CL-20 found in the cocrystal divided by the CL-20 needed to reach TP1.

Table 4. Theoretical maximum cocrystal yields and CL-20 efficiencies for cooling and antisolvent crystallisation at 60 °C in different solvents.

	cocrystal yield (g _{cocrystal} /g _{solvent})	CL-20 efficiency (%)
ACN	0.22	38
cyclohexanone	0.06	7
propylene carbonate	0.24	48

Given that the cocrystal yields and the CL-20 efficiencies are hypothetical limit values that in practice cannot be achieved [22], cyclohexanone is deemed unfit for antisolvent and cooling crystallisation, due to the low CL-20 efficiency. At best for every gram of CL-20 found in the cocrystal more than ten grams of CL-20 remain in solution.

In batch RC excess CL-20 and HMX is used. In a very simplified manner the crystallisation process follows the double arrow B in Figure 2. The excess reactants are constantly dissolved while the cocrystal crystallises. The cocrystal yield is therefore not directly dependent on the cocrystal solubility curve, but on the excess of reactant. In Table 5 cocrystal yields and CL-20 efficiencies for an excess of 0.5 g and 1 g reactant mixture per g solvent are presented for the three solvents.

The CL-20 efficiency values in Table 5 clearly indicate that for RC the position of TP1 and the corresponding solubility ratio are of less importance compared with antisolvent and cooling crystallisation. In addition, higher cocrystal yields and CL-20 efficiencies are achievable.

Table 5. Cocrystal yields and CL-20 efficiencies for RC at 60 °C in different solvents and different solid excess.

	cocrystal yield (g _{cocrystal} /g _{solvent})		CL-20 efficiency (%)	
	xs 0.5 g/g	xs 1 g/g	xs 0.5 g/g	xs 1 g/g
ACN	0.5	1	63	85
cyclohexanone	0.5	1	51	74
propylene carbonate	0.5	1	67	89

For evaporation crystallisation both TP1 and TP2 are of relevance, because in all tested solvents the cocrystal is more soluble than HMX. During evaporation and the resulting crystallisation of cocrystal, the solution concentration of CL-20 therefore increases. The endpoint of the evaporation crystallisation is therefore determined by TP2. Due to its superior solvent properties TP2 was only determined for ACN. The theoretical cocrystal yield and CL-20 efficiency are 0.22 g cocrystal per g ACN and 38% respectively.

The phase diagrams for ACN, ACN/2-propanol, propylene carbonate and propylene carbonate/2-propanol are provided in the supporting information.

3.2 Crystallisation Experiments

3.2.1 Antisolvent Crystallisation

Antisolvent experiments were carried out in ACN at 60 °C with 2-propanol as antisolvent. To ensure that the solution composition does not exit the cocrystal phase region it is beneficial to determine the PSD for the starting and end solvent mixture. The PSD for CL-20 and HMX in ACN and ACN/2-propanol (1:1 mass ratio) and the solution compositions during the crystallisation are presented in Figure 3. The solution composition trajectory in antisolvent crystallisation differs from the trajectory in cooling crystallisation because over the course of the antisolvent crystallisation experiment the solution volume increases, which consequently also changes the concentration of CL-20 and HMX. Figure 3 shows that for this 2-propanol fraction the final solution composition would be close to TP2 and CL-20 might crystallise. A ratio of 3:2 ACN to 2-propanol was therefore chosen as the final solvent composition.

Following this procedure the cocrystal yield achieved is 0.166 g cocrystal per g ACN and the CL-20 efficiency is 25%. Cocrystals with a width-to-height ratio between 2 and 1.2

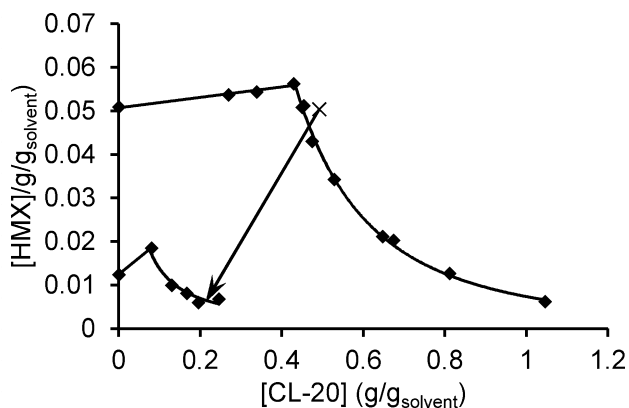


Figure 3. The arrow visualises the crystallisation path in the PSD for antisolvent crystallisations in ACN at 60 °C. X indicates the starting solution composition.

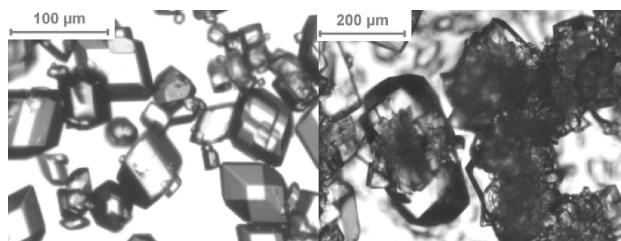


Figure 4. Cocrystal obtained from unseeded antisolvent crystallisation in ACN at 60 °C.

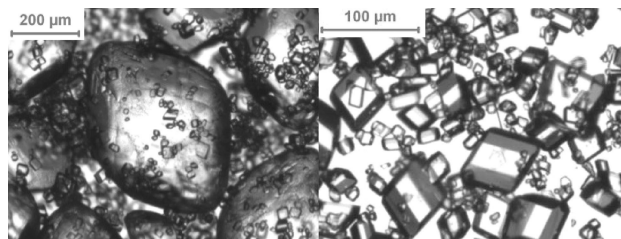


Figure 5. Coarse cocrystal formed over 24 h with finer cocrystals formed during the self-seeded antisolvent crystallisation in ACN at 60 °C (left). Cocrystals formed during the self-seeded antisolvent crystallisation in ACN at 60 °C (right).

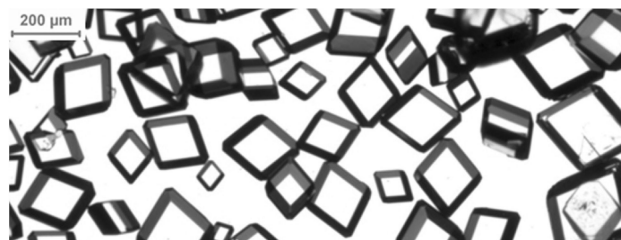


Figure 6. Cocrystal formed in externally-seeded antisolvent crystallisation in ACN at 60 °C.

were obtained. The width-to-height ratio did not exhibit a correlation to the controlled crystallisation parameters. Three seeding strategies were explored: no seeding, self-seeding and the addition of seed crystals. Macroscopic images of three representative crystal batches are shown in Figures 4–6.

In unseeded crystallisation experiments conducted in parallel, in some reaction mixtures randomly malformed cocrystals occurred (Figure 4, right). Furthermore, no reproducible crystal sizes were obtained.

The self-seeding experiments reveal that within the metastable region slow nucleation of the cocrystal occurs. This procedure produced high-quality cocrystals; however, it is inefficient in producing cocrystals with a defined crystal size distribution. On the one hand, the initial supersaturation is used up to produce unusably large crystals in the range of 700 µm, which reduces the cocrystal yield by 36 mg g⁻¹, and on the other hand, due to the random na-

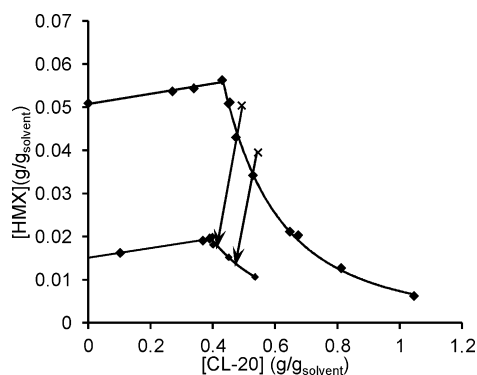


Figure 7. Arrows visualise the crystallisation path in the PSD for cooling crystallisations in ACN from 60 °C to 20 °C. X indicates the starting solution compositions.

ture of nucleation and the following abrasion, the number of seed crystals and therefore the final size distribution of the cocystal cannot be controlled.

To control the final crystal size, external seeding was applied. To reduce crystal defects on the surface and the amount of internal defects of the seed crystals, the seed crystals were about 90% dissolved prior to use. This serves the additional purpose of reducing the fines among the seed crystals and effectively narrowing down the seed crystal size distribution. Assuming that the seeds have a uniform size, that no nucleation and breakage occurs, and that all material crystallises on the seed crystals, the required seed crystal mass m_{seed} can be calculated using the seed crystal size l_{seed} the desired final crystal size l_{final} and the cocystal yield m_{final} [23]:

$$m_{\text{seed}} = m_{\text{final}} \cdot (l_{\text{seed}}/l_{\text{final}})^3$$

Under experimental conditions this equation can only function as a guideline and the appropriate seed crystal mass has to be determined experimentally. For the laboratory-scale experiments it was found that 25% of the calculated seed crystal mass was needed to obtain an l_{final} of around 200 μm using seed crystals with $d_m = 33.2 \mu\text{m}$.

Unseeded antisolvent crystallisation was also carried out with propylene carbonate as solvent in order to determine whether, under more controlled conditions, more compact crystals can be produced. However, no improvement was achieved compared to the initially obtained value (Table 2). No further experiments were carried out with propylene carbonate.

3.2.2 Cooling Crystallisation

Externally seeded cooling crystallisations were carried out in ACN from 60 °C to 20 °C. It was found that crystallisations with the same solution composition as the antisolvent crystallisations only produced pure cocystal in about 50% of

the batches. Of six cooling crystallisations conducted in parallel, two to four typically produced fluctuating amounts of HMX and cocystal, while the others produced pure cocystal. It is reasonable to assume that the close vicinity of the solution composition to the HMX phase region during the crystallisation facilitated the HMX crystallisation. This is supported by the finding that in one PSD experiment of ACN at 60 °C multiple solutions with a solution composition in the cocystal phase region near the boundary to the HMX phase region exhibited non-equilibrium conditions after 5 days, which indicates that initially all cocystal was dissolved and HMX recrystallised. To prevent HMX impurities the solution composition was adapted to proceed further in the middle of the phase region (Figure 7).

Linear cooling from 60 °C to 20 °C within 16.6 h resulted in an average cocystal yield of 34 mg/g which is only 34% of the expected yield of 101 mg/g. This indicates that under similar conditions as the antisolvent crystallisation, cooling crystallisation exhibits lower conversion rates. Total crystallisation was achieved with a cooling rate resembling natural cooling within 25 h. Cocystals with a width-to-height ratio of 1 were obtained.

3.2.3 Batch Reaction CocrySTALLIZATION

Batch RC in an intermediate scale was carried out at 60 °C with ACN and cyclohexanone. Total conversion occurred in ACN within 1 h. Cyclohexanone, however, required the addition of seed crystals, because after 3 h no conversion occurred. Total conversion was achieved within 18 h. This indicates that the total solubility of CL-20 and HMX in cyclohexanone is insufficient to create a nucleation shower, whereas in ACN fast nucleation occurs. 60 °C was chosen for cooling and antisolvent crystallisation to maximise the cocystal yield and CL-20 efficiency. For RC, however, the solubility is of lesser importance. Thus, 20 °C might also be a viable temperature for RC. Due to excessive viscosity no RC at 20 °C was carried out in cyclohexanone. In ACN, of two identical reaction mixtures, one produced pure irregularly shaped cocystal within 2 h, whereas the other was interrupted after 18 h, at which point the solid was composed of a mixture of ϵ CL-20, β CL-20, α CL-20 and β HMX. Intermittently gathered samples indicate that at 10 min and 5.5 h reaction time small amounts of cocystal were formed, however no cocystal was present in the samples between 10 min and 5 h. To reduce the number of factors that might contribute to this discrepancy, laboratory-scale seeded and unseeded RC were carried out in parallel. Of the five seeded reaction mixtures, two were incompletely transformed, whereas all four unseeded reaction mixtures were incompletely transformed after 24 h. After 48 h, all seeded and none of the unseeded reaction mixtures were completely transformed. It is likely that the low conversion rate and the appearing and disappearing of cocystal at 20 °C in ACN is the result of a lower energy benefit of crystallising

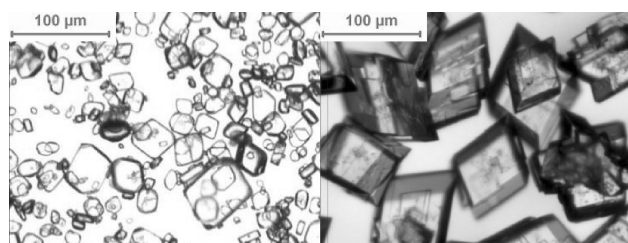


Figure 8. Cocrystals formed in intermediate-scale seeded batch RC in cyclohexanone at 60 °C (left) and cocrystals formed in intermediate-scale batch RC in ACN at 60 °C (right).

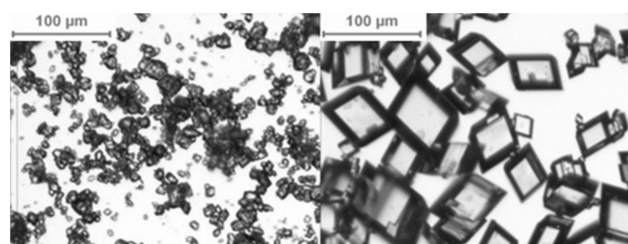


Figure 9. Cocrystals formed in intermediate-scale batch RC in ACN at 20 °C (left). Cocrystals formed in laboratory-scale batch RC in ACN at 20 °C (right).

cocrystal compared to crystallising CL-20 and HMX at 20 °C compared to 60 °C and a therefore more labile cocrystal phase region.

As can be seen in Figure 8 (left) and Figure 9 (right), good crystal quality is obtained in both seeded experiments. However, both d_m with 39 µm and 45 µm for the cyclohexanone and ACN experiment are far smaller than the seeding should account for. This shows that m_{seed} must be adjusted specifically to the reaction condition, since after long reaction times nucleation and attrition have likely occurred in these experiments. More defects are visible in the cocrystals obtained from intermediate-scale batch RC in ACN at 60 °C which might be caused by the much higher crystallisation rate. The obtained d_m was 83 µm. The width-to-height ratios for batch RC in ACN at 60 °C, 20 °C laboratory-scale and cyclohexanone are 1.4, 1.2 and 2.2 respectively.

Based on the varying results for batch RC in ACN at 20 °C and the higher width-to-height ratio in cyclohexanone, ACN at 60 °C was chosen as the best condition to produce fine cocrystal. A batch RC scale-up in ACN at 60 °C was undertaken. By directly recycling the reaction solution after solid-liquid-separation, 253 g cocrystal with a combined d_m of 33 µm [24] and width-to-height ratio of 2.7 was produced in three consecutive batches with a CL-20 efficiency of 79%. The difference in particle diameter and width-to-height ratio compared to the previous experiment shows that the size and morphology of the obtained crystals seems to be significantly dependent on the crystallisation conditions.

3.2.4 Evaporation Crystallisation

No evaporation crystallisation was carried out, because no higher CL-20 efficiency and crystal quality is to be expected compared to antisolvent crystallisation. Unlike in antisolvent and cooling crystallisation the theoretical values for cocrystal yield and CL-20 efficiency can be achieved. This, however, requires the crystallisation to start at TP1 and end at TP2. In the beginning phase as well as the final phase of the crystallisation, the solution composition is very close to the phase boundaries, which can facilitate the crystallisation of HMX and CL-20. A more robust evaporation crystallisation in ACN, starting at the same solution composition as the antisolvent crystallisations and ending at the solution composition of 0.90 g CL-20 per g ACN and 0.01 g HMX per g ACN would yield 0.19 g cocrystal per g ACN and a CL-20 efficiency of 26% which is insignificantly better than the values achieved for antisolvent crystallisation.

4 Conclusion

It was found that the solubility ratio of the individual cocrystal components serves as a basic tool for roughly judging the achievable cocrystal yield; however, the position of TP1 cannot be predicted based solely on the solubility data for the pure substances. Furthermore, most tested solvents produced cocrystals of undesirable morphology.

In summary, ACN remains the only utilisable solvent of those tested that produces compact CL-20/HMX cocrystal, even though the solubility ratio at TP1 is far from ideal. As a consequence, while antisolvent and cooling crystallisation are capable of producing high quality cocrystal, they suffer from an insufficient CL-20 efficiency and, in the case of antisolvent crystallisation, additionally from a difficult recycling of the non-crystallised explosive. Batch RC exhibits good CL-20 efficiency, but at temperatures of 60 °C batch RC gives no control over the product crystal size, and at 20 °C batch RC leads to varying crystallisation.

Thus, none of the tested crystallisation methods fulfils all of the proposed specifications (Table 6). However, one possible approach to meet the specifications might be to find an intermediate temperature between 20 °C and 60 °C for batch RC, where nucleation and crystal growth rate are

Table 6. Summary of crystal quality, crystal size, CL-20 efficiency and solution recyclability for different crystallisation methods and conditions.

crystallisation method	crystal quality	200 µm possible	CL-20 efficiency	solution recyclability
antisolvent	+	Yes	25 %	–
cooling	+	Yes	14 %	+
RC at 60 °C	–	No	> 75 %	+
RC at 20 °C	+ / –	yes	> 70 %	++

still low but the cocrystal is thermodynamically more favoured and therefore more reliably formed. Another solution might be semi-batch reaction crystallisation, where HMX and CL-20 are dosed into the reaction mixture as the crystallisation progresses, thereby keeping the supersaturation on a low level, preventing nucleation and reducing the crystal growth rate. In the course of these experiments the factors influencing the fluctuating width-to-height ratios must also be uncovered. Although the specifications have not yet been met, pure cocrystal with moderate crystal quality and a d_m applicable in PBX can be obtained by batch RC in a reasonable scale. Valuable data can be collected by using this material in PBX test charges.

Acknowledgements

We are grateful for financial support provided by the German Ministry of Defense and the support provided by Dr. Manfred Kaiser at the WTD91.

References

- [1] R. L. Simpson, P. A. Urtiew, D. L. Ornellas, G. L. Moody, K. J. Scribner, D. M. Hoffman, CL-20 performance exceeds that of HMX and its sensitivity is moderate, *Propellants Explos. Pyrotech.* **1997**, 22, 5, 249–255
- [2] U. R. Nair, R. Sivabalan, G. M. Gore, M. Geetha, S. N. Asthana, H. Singh, Hexanitrohexaazaisowurtzitane (CL-20) and CL-20-based formulations, *Combust. Explos. Shock Waves* **2005**, 41, 2, 121–132.
- [3] O. Bolton, L. R. Simke, P. F. Pagoria, A. J. Matzger, High Power Explosive with Good Sensitivity: A 2:1~Cocrystal of CL-20:HMX, *Cryst. Growth Des.* **2012**, 12, 9, 4311–4314
- [4] N. C. Johnson, CL-20 Sensitivity Round Robin, Report IHSP 03-487, *Indian Head Division Naval Surface Warfare Center*, Indian Head, MD, USA **2003**.
- [5] S. Aitipamula, R. Banerjee, A. K. Bansal, K. Biradha, M. L. Cheney, A. R. Choudhury, G. R. Desiraju, A. G. Dikundwar, R. Dubey, N. Duggirala, P. P. Ghogale, S. Ghosh, P. K. Goswami, N. R. Goud, R. R. K. Jeti, P. Karpinski, P. Kaushik, D. Kumar, V. Kumar, B. Moulton, A. Mukherjee, G. Mukherjee, A. S. Myerson, V. Puri, A. Ramanan, T. Rajamannar, C. M. Reddy, N. Rodriguez-Hornedo, R. D. Rogers, T. N. G. Row, P. Sanphui, N. Shan, G. Shete, A. Singh, C. C. Sun, J. A. Swift, R. Thaimattam, T. S. Thakur, R. K. Thaper, S. P. Thomas, S. Tothadi, V. R. Vangala, N. Variankaval, P. Vishweshwar, D. R. Weyna, M. J. Zaworotko, 'Polymorphs, Salts, and Cocrystals: What's in a Name?', *Cryst. Growth Des.* **2012**, 12, 5, 2147–2152
- [6] a) G. R. Desiraju, Crystal and co-crystal, *CrystEngComm* **2003**, 5, 82, 466; b) P. Vishweshwar, J. A. McMahon, J. A. Bis, M. J. Zaworotko, Pharmaceutical Co-Crystals, *J. Pharm. Sci.* **2006**, 95, 3, 499–516; c) S. L. Childs, G. P. Stahly, A. Park, The Salt-Cocrystal Continuum: ~ The Influence of Crystal Structure on Ionization State, *Mol. Pharmaceutics* **2007**, 4, 3, 323–338; d) A. D. Bond, What is a co-crystal?, *CrystEngComm* **2007**, 9, 9, 833; e) G. P. Stahly, Diversity in Single- and Multiple-Component Crystals. The Search for and Prevalence of Polymorphs and Cocrystals, *Cryst. Growth Des.* **2007**, 7, 6, 1007–1026; f) S. Mohamed, D. A. Tocher, M. Vickers, P. G. Karamertzanis, S. L. Price, Salt or Cocrystal? A New Series of Crystal Structures Formed from Simple Pyridines and Carboxylic Acids, *Cryst. Growth Des.* **2009**, 9, 6, 2881–2889.
- [7] S. R. Anderson, D. J. am Ende, J. S. Salan, P. Samuels, Preparation of an Energetic-Energetic Cocrystal using Resonant Acoustic Mixing, *Propellants Explos. Pyrotech.* **2014**, 39, 5, 637–640
- [8] D. Spitzer, B. Risse, F. Schnell, V. Pichot, M. Klauwünzer, M. R. Schaefer, Continuous engineering of nano-cocrystals for medical and energetic applications, *Sci. Rep.* **2014**, 4, 6575
- [9] C. An, H. Li, B. Ye, J. Wang, Nano-CL-20/HMX Cocrystal Explosive for Significantly Reduced Mechanical Sensitivity, *J. Nanomater.* **2017**, 2017, 1–7
- [10] S. Sun, H. Zhang, Y. Liu, J. Xu, S. Huang, S. Wang, J. Sun, Transitions from Separately Crystallized CL-20 and HMX to CL-20/HMX Cocrystal Based on Solvent Media, *Cryst. Growth Des.* **2018**, 18, 1, 77–84.
- [11] M. Gosh, A. K. Sikder, S. Banerjee, R. G. Gonnade, Studies on CL-20/HMX (2:1) Cocrystal: A New Preparation Method and Structural and Thermokinetic Analysis, *Cryst. Growth Des.* **2018**, 7, 3781–3793
- [12] B. Gao, W. Dunju, J. Zhang, Y. Hu, J. Shen, J. Wang, B. Huang, Z. Qiao, H. Huang, F. Nie, G. Yang, Facile, continuous and large-scale synthesis of CL-20/HMX nano co-crystals with high-performance by ultrasonic spray-assisted electrostatic adsorption method, *J. Mater. Chem. A* **2014**, 2, 19969–19974
- [13] H. Qiu, R. B. Patel, R. S. Damavarapu, V. Stepanov, Nanoscale 2CL-20/HMX high explosive cocrystal synthesized by bead milling, *CrystEngComm* **2015**, 17, 22, 4080–4083
- [14] N. Rodríguez-Hornedo, S. J. Nehm, K. F. Seefeldt, Y. Pagán-Torres, C. J. Falkiewicz, Reaction Crystallization of Pharmaceutical Molecular Complexes, *Mol. Pharmaceutics* **2006**, 3, 3, 362–367
- [15] a) J. E. Field, Hot spot ignition mechanisms for explosives, *Acc. Chem. Res.* **1992**, 25, 11, 489–496; b) Menikoff, R., Pore Collapse and Hot Spots in HMX, *AIP Conf. Proc.*, Portland, Oregon, USA, July 20–25, **2003** p 393–396; c) R. H. B. Bouma, W. Duvalois, A. E. D. M. van der Heijden, Microscopic characterization of defect structure in RDX crystals, *J. Microsc.* **2013**, 252, 3, 263–274; d) S. M. Walley, J. E. Field, M. W. Greenaway, Crystal sensitivities of energetic materials, *Mater. Sci. Technol.* **2006**, 22, 4, 402–413; e) L. Borne, J.-C. Patedoye, C. Spyckerelle, Quantitative Characterization of Internal Defects in RDX Crystals, *Propellants Explos. Pyrotech.* **1999**, 24, 4, 255–259
- [16] a) D. H. Leung, S. Lohani, R. G. Ball, N. Canfield, Y. Wang, T. Rhodes, A. Bak, Two Novel Pharmaceutical Cocrystals of a Development Compound – Screening, Scale-up, and Characterization, *Cryst. Growth Des.* **2012**, 12, 3, 1254–1262; b) R. A. Chiarella, R. J. Davey, M. L. Peterson, Making Co-Crystals The Utility of Ternary Phase Diagrams, *Cryst. Growth Des.* **2007**, 7, 7, 1223–1226; c) S. Kudo, H. Takiyama, Production method of carbamazepine/saccharin cocrystal particles by using two solution mixing based on the ternary phase diagram, *J. Cryst. Growth* **2014**, 392, 87–91; d) S. Boyd, K. Back, K. Chadwick, R. J. Davey, C. C. Seaton, Solubility Metastable Zone Width Measurement and Crystal Growth of the 1:1~Benzoic Acid/Isonicotinamide Cocrystal in Solutions of Variable Stoichiometry, *J. Pharm. Sci.* **2010**, 99, 9, 3779–3786; e) X. Sun, Q. Yin, S. Ding, Z. Shen, Y. Bao, J. Gong, B. Hou, H. Hao, Y. Wang, J. Wang, C. Xie, (Solid + liquid) phase diagram for (indomethacin + nicotinamide)-methanol or methanol/ethyl acetate mixture and solubility behavior of 1:1 (indomethacin + nicotinamide) co-crystal at T=(298.15 and 313.15) K, *J. Chem. Thermodyn.* **2015**, 85, 171–177

- [17] D. J. Good, N. Rodríguez-Hornedo, Solubility Advantage of Pharmaceutical Cocrystals, *Cryst. Growth Des.* **2009**, *9*, 5, 2252–2264
- [18] a) E. von Holtz, D. Ornellas, M. F. Foltz, J. E. Clarkson, The Solubility of ϵ -CL-20 in Selected Materials *Propellants Explos. Pyrotech.* **1994**, *19*, 4, 206–212; b) Y. T. Lapina, A. S. Savitskii, E. V. Motina, N. V. Bychin, A. A. Lobanova, N. I. Golovina, Polymorphic transformations of hexanitrohexaazaisowurtzitane, *Russ. J. Appl. Chem.* **2009**, *82*, 10, 1821–1828; c) L. Svensson, J.-O. Nyqvist, L. Westling, Crystallization of HMX from γ -butyrolactone, *J. Hazard. Mater.* **1986**, *13*, 1, 103–108; d) J. F. Baytos, B. G. Craig, A. W. Campbell, W. E. Deal, J. J. Dick, R. H. Dinegar, R. P. Engelke, T. E. Larson, E. Marshall, J. B. Ramsay, R. N. Rogers, D. Soran, M. J. Urizar, J. D. Wackerle, *LASL explosive property data* (Eds.: T. R. Gibbs, A. Popolato), Univ of California Press, Berkeley **1980**, p.44; e) M. E. Sitzmann, S. Foti, C. C. Misener, *Solubilities of high explosives: removal of high explosive fillers from munitions by chemical dissolution*, Naval Ordnance Lab, White Oak, MD, USA, **1973**.
- [19] SNPE Safety Data Sheet
- [20] a) A. K. Tiwary, Modification of Crystal Habit and Its Role in Dosage Form Performance, *Drug Dev. Ind. Pharm.* **2001**, *27*, 7, 699–709; b) S. Li, J. Xu, G. Luo, Control of crystal morphology through supersaturation ratio and mixing conditions, *J. Cryst. Growth* **2007**, *304*, 1, 219–224
- [21] a) A. Alhalaweh, A. Sokolowski, N. Rodríguez-Hornedo, S. P. Velaga, Solubility Behavior and Solution Chemistry of Indomethacin Cocrystals in Organic Solvents, *Cryst. Growth Des.* **2011**, *11*, 9, 3923–3929; b) S. L. Childs, N. Rodríguez-Hornedo, L. S. Reddy, A. Jayasankar, C. Maheshwari, L. McCausland, R. Shipplett, B. C. Stahly, Screening strategies based on solubility and solution composition generate pharmaceutically acceptable cocrystals of carbamazepine, *CrystEngComm* **2008**, *10*, 7, 856
- [22] By applying high initial supersaturations it is theoretically possible to surpass these values; however, these supersaturations are of no practical use in the described crystallisation experiments.
- [23] A. H. Janse, **1977**, Nucleation and crystal growth in batch crystallizers, *PhD Thesis*, Delft, Netherlands
- [24] Laser diffraction measurements are found in the supporting information.

Manuscript received: October 24, 2018

Revised manuscript received: January 18, 2019

Version of record online: March 19, 2019